Structural basis of outer dynein arm intraflagellar transport by the transport adaptor protein ODA16 and the intraflagellar transport protein IFT46

Received for publication, February 6, 2017, and in revised form, March 3, 2017 Published, Papers in Press, March 15, 2017, DOI 10.1074/jbc.M117.780155

Michael Taschner[‡1], **André Mourão**[§1], **Mayanka Awasthi**[¶1], **Jerome Basquin**[‖], **and Esben Lorentzen**[‡2]

From the [‡]*Department of Molecular Biology and Genetics, Aarhus University, DK-8000 Aarhus C, Denmark, the* [§]*Institute of Structural Biology, Helmholtz Zentrum München, 85764 Neuherberg, Germany, the* [¶]*Department of Cell Biology and Molecular Genetics, University of Maryland, College Park, Maryland 20742, and the* [‖]*Department of Structural Cell Biology, Max-Planck-Institute of Biochemistry, D-82152 Martinsried, Germany*

Edited by Joseph Jez

Motile cilia are found on unicellular organisms such as the green alga *Chlamydomonas reinhardtii*, on sperm cells, and on cells that line the trachea and fallopian tubes in mammals. The motility of cilia relies on a number of large protein complexes including the force-generating outer dynein arms (ODAs). The transport of ODAs into cilia has been previously shown to require the transport adaptor ODA16, as well as the intraflagellar transport (IFT) protein IFT46, but the molecular mechanism by which ODAs are recognized and transported into motile cilia is still unclear. Here, we determined the high-resolution crystal structure of *C. reinhardtii* ODA16 (CrODA16) and mapped the binding to IFT46 and ODAs. The CrODA16 structure revealed a small 80-residue N-terminal domain and a C-terminal 8-bladed β-propeller domain that are both required for the association with the N-terminal 147 residues of IFT46. The dissociation constant of the IFT46-ODA16 complex was 200 nM, demonstrating that CrODA16 associates with the IFT complex with an affinity comparable with that of the individual IFT subunits. Furthermore, we show, using ODAs extracted from the axonemes of *C. reinhardtii*, that the C-terminal β-propeller but not the N-terminal domain of CrODA16 is required for the interaction with ODAs. These data allowed us to present an architectural model for ODA16-mediated IFT of ODAs.

Cilia are organelles that protrude from the surface of eukaryotic cells to serve a number of functions in cell motility, sensory reception, and developmental signaling. Motile cilia are the cellular machines that propel unicellular organisms through aqueous media (1). They are also vital for human health because they drive the mucociliary flow to remove inhaled pathogens from the airways, move egg cells through the fallopian tubes to reach the uterus, and drive the left-right asymmetry during development, which is required for the correct positioning of inner organs (2). It is thus not surprising that mutations causing absence or defects in motile cilia result in diseases and disorders categorized as primary cilia dyskinesia (3, 4).

Primary and motile cilia adopt the same slender hair-like appearance and share a microtubule-based axoneme surrounded by a ciliary membrane (5). They do, however, differ in the presence of a number of motility complexes found only in the axoneme of motile cilia. These include outer dynein arms (ODAs),[3] which are large ATPase complexes that, together with several inner dynein arms, power the bending of cilia required for cilium-mediated motility (6). ODAs are MDa-sized multisubunit complexes that preassemble in the cytoplasm before trafficking into the cilium (7). Four ODAs are found within the 96-nm repeat of the axoneme, where they attach stably to the A tubule of the microtubule doublets and transiently interact with the B-tubule to cause bending of the axoneme resulting in motility (8–12).

Several high-resolution structures have recently shed light onto the molecular mechanisms of dynein motors (13–15). Less is known about the molecular basis of how ODAs are recognized and transported into the axonemes of motile cilia. This trafficking process is, however, known to require the adaptor protein ODA16, which was discovered through the characterization of a *C. reinhardtii oda16* mutant displaying reduced beat frequency and altered swimming behavior because of a partial loss of axonemal ODAs (16). ODA16 is a predicted WD protein conserved only in organisms with motile cilia (WDR69 in human, 62% sequence identity to the *C. reinhardtii* protein (16)) and is also required for proper motile cilium function in zebrafish (17).

A more detailed picture of the molecular function of ODA16 emerged when it was discovered that ODA16 acts in ODA transport through an interaction with the intraflagellar transport (IFT) machinery (18, 19). IFT is an evolutionarily conserved process (20, 21) that moves proteinacious particles bidirectionally inside cilia to deliver axonemal building blocks such as tubulin to the tip of cilia (22–26). IFT relies on a 22-subunit IFT complex that organizes into a 16-subunit IFT-B and a 6-subunit IFT-A complex (27–29). The 16-subunit IFT-B com-

This work was supported by Novo Nordisk Foundation Grant NNF15OC0014164 and European Research Council Grant 310343. The authors declare that they have no conflicts of interest with the contents of this article.

The atomic coordinates and structure factors (code 5MZH) have been deposited in the Protein Data Bank (http://wwpdb.org/).

This article contains supplemental Figs. S1–S3.

[1] These authors contributed equally to this work.

[2] To whom correspondence should be addressed. E-mail: el@mbg.au.dk.

[3] The abbreviations used are: ODA, outer dynein arm; IFT, intraflagellar transport; SEC, size exclusion chromatography; ITC, isothermal titration calorimetry; fl, full-length; SAXS, small-angle X-ray scattering.

© 2017 by The American Society for Biochemistry and Molecular Biology, Inc. Published in the U.S.A.

Downloaded from http://www.jbc.org/ at Helmholtz Zentrum Muenchen - Zentralbibliothek on June 13, 2017

plex can be further subdivided into a 10-subunit IFT-B1 subcomplex and a 6-subunit IFT-B2 subcomplex (30–32), both of which can be reconstituted and purified separately (31, 33). IFT46 is an IFT-B1 subunit that is necessary for IFT complex assembly through an interaction of its C-terminal domain with IFT52, another IFT-B1 subcomplex component (33–35). IFT46 was shown to interact directly with ODA16 (18) and to be required for the transport of ODAs into cilia (19). Whereas the *ift46* null mutant is unable to assemble flagella, likely because of a failure in IFT complex formation, a suppressor strain that alleviates this "no cilia" phenotype of *ift46* was isolated and shown to have full-length cilia that specifically lack ODAs. This *ift46* suppressor mutant likely expresses the C-terminal domain of IFT46 required for IFT complex formation but lacks the N-terminal region of IFT46, suggesting that the ODA16 interacting domain is found within this region of IFT46 (19).

Here we purified recombinantly produced ODA16 and ODA16-IFT46 complexes of the biflagellate green alga *C. reinhardtii* and dissected the molecular basis of the IFT46-ODA16-ODA interaction underlying the ciliary trafficking of ODAs. We determined the high-resolution crystal structure of ODA16 and mapped the interaction with ODAs and IFT46 using biochemical and biophysical methodology. The results show that ODAs associate with the C-terminal ODA16 β-propeller, whereas IFT46-interaction requires the small 80-residue N-terminal domain of ODA16.

Results

ODA16 binds directly to the N-terminal 147 residues of IFT46

Previously published yeast two-hybrid and pulldown analysis revealed an interaction between ODA16 and IFT46 (18). Furthermore, analysis of an IFT46 suppressor strain suggested that the N-terminal region of IFT46 is responsible for the IFT of ODAs (19). To analyze the ODA16-IFT46 association using direct protein-protein interaction assays, we purified recombinant ODA16 (Fig. 1, *a* and *b*) and GST-IFT46 (all proteins used in this study are of the green alga *C. reinhardtii*) and carried out pulldown experiments, which revealed a strong ODA16-IFT46 interaction (Fig. 1*c*). The ODA16-IFT46 complex appears stoichiometric at 200 mM NaCl, but the complex gradually falls apart when the salt concentration is increased to 1 M (Fig. 1*c*), suggesting at least a partly hydrophilic mode of association. Size exclusion chromatography (SEC) of IFT46, ODA16, or an equimolar mixture of the two proteins in 200 mM NaCl demonstrated the formation of a stable complex (Fig. 1*d*). Whereas ODA16 elutes from SEC close to the position of a globular protein, IFT46 elutes at a significantly smaller volume, suggesting an elongated shape. This is consistent with the predicted modular multidomain organization, as well as with the presence of a long flexible region (Figs. 1*d* and 2*a* and supplemental Fig. S1). To quantify the affinity of the ODA16-IFT46 interaction, we titrated purified untagged ODA16 with untagged IFT46 in isothermal titration calorimetry (ITC) experiments. The result shown in Fig. 1*e* demonstrates that ODA16-IFT46 forms a stoichiometric complex ($n = 0.96$) with a dissociation constant (K_d) of 217 nM in agreement with the stable complex formation observed in SEC. The affinity of ODA16 for IFT46 is thus similar to that observed between IFT subunits, suggesting that ODA16 could be an integral subunit of the IFT-B complex during cilium formation (Refs. 31, 33, and 34 and data not shown).

To map the domain(s) of IFT46 required for association with ODA16, we carried out binding studies with truncated versions of IFT46. The C-terminal domain of IFT46 associates with IFT52, is required for the formation of the IFT-B1 complex (33–35), and rescues the more severe ciliogenesis phenotype observed in the *ift46 C. reinhardtii* mutant but not the lack of axonemal ODAs (19). In agreement with these data, $IFT46_{147\text{-}C}$ (IFT46C) did not co-elute with ODA16 in SEC (Fig. 2*b*). Consistently, IFT46C did not show any detectable interaction with ODA16 in ITC experiments, suggesting that the association, if any, is at least 2 orders of magnitude weaker than for full-length (fl) IFT46 (Fig. 2*c*). To probe the interaction between the N-terminal $IFT46_{1-147}$ region (IFT46N) and ODA16, the two proteins were incubated and applied to SEC, which demonstrated a stable ODA16-IFT46N complex (Fig. 2*d*). To assess the interaction quantitatively, ODA16 was titrated with IFT46N in ITC, revealing a stoichiometric complex ($n = 1.08$) with a K_d of 247 nM (Fig. 2*e*). IFT46 (fl) and IFT46N thus interact with ODA16 with similar affinities (difference in K_d is smaller than 1 standard deviation; see Figs. 1*e* and 2*e*). This indicates that the IFT46N construct contains the entire ODA16-binding region. We were unable to carry out a more detailed mapping of the IFT46N construct, because shorter IFT46 fragments tested were either insoluble or not expressed (data not shown). We conclude that residues 1–147 of IFT46 interact with nanomolar affinity with the ODA cargo-adaptor ODA16.

Crystal structure of ODA16

All protein constructs and complexes shown in Figs. 1 and 2 were screened for crystallization, which resulted in crystal hits for ODA16 but not IFT46 (fl or N) or ODA16-IFT46 complexes. X-ray diffraction data at 2.4 Å resolution together with the molecular replacement model of an eight-bladed β-propeller structure from the ribosomal assembly factor 4 (RSA4; PDB code 4wjs) were used to determine the three-dimensional structure of ODA16 (Fig. 3 and Table 1). Full-length ODA16 was crystallized, and the resulting map had visible electron density for both the smaller ~80 residue N-terminal domain (ODA16N) and the β-propeller but not for the most ~25 C-terminal residues that are presumably disordered (Figs. 1*a* and 3*a* and supplemental Fig. S2). The N-terminal ODA16 domain folds into a three-stranded anti-parallel β-sheet followed by two α-helices that connect to the C-terminal β-propeller domain via a seven-residue linker region (Fig. 3*a*). This linker region together with residues from two loop regions (amino acids 13–15 and 33–36) of ODA16N interact with residues from loop regions of the N-terminal face of the β-propeller to position the two domains relative to each other via a rather small interface (Fig. 3*b*). ODA16N shows structural similarity to domains found in otherwise functionally unrelated proteins such as the Ser/Thr kinase WNK1 (PDB code 2lru) and the ribosomal proteins UL2 and UL12 (PDB codes 4w20 and 1vx1) (36, 37). The protein structure in the PDB most similar to the

Downloaded from http://www.jbc.org/ at Helmholtz Zentrum Muenchen - Zentralbibliothek on June 13, 2017

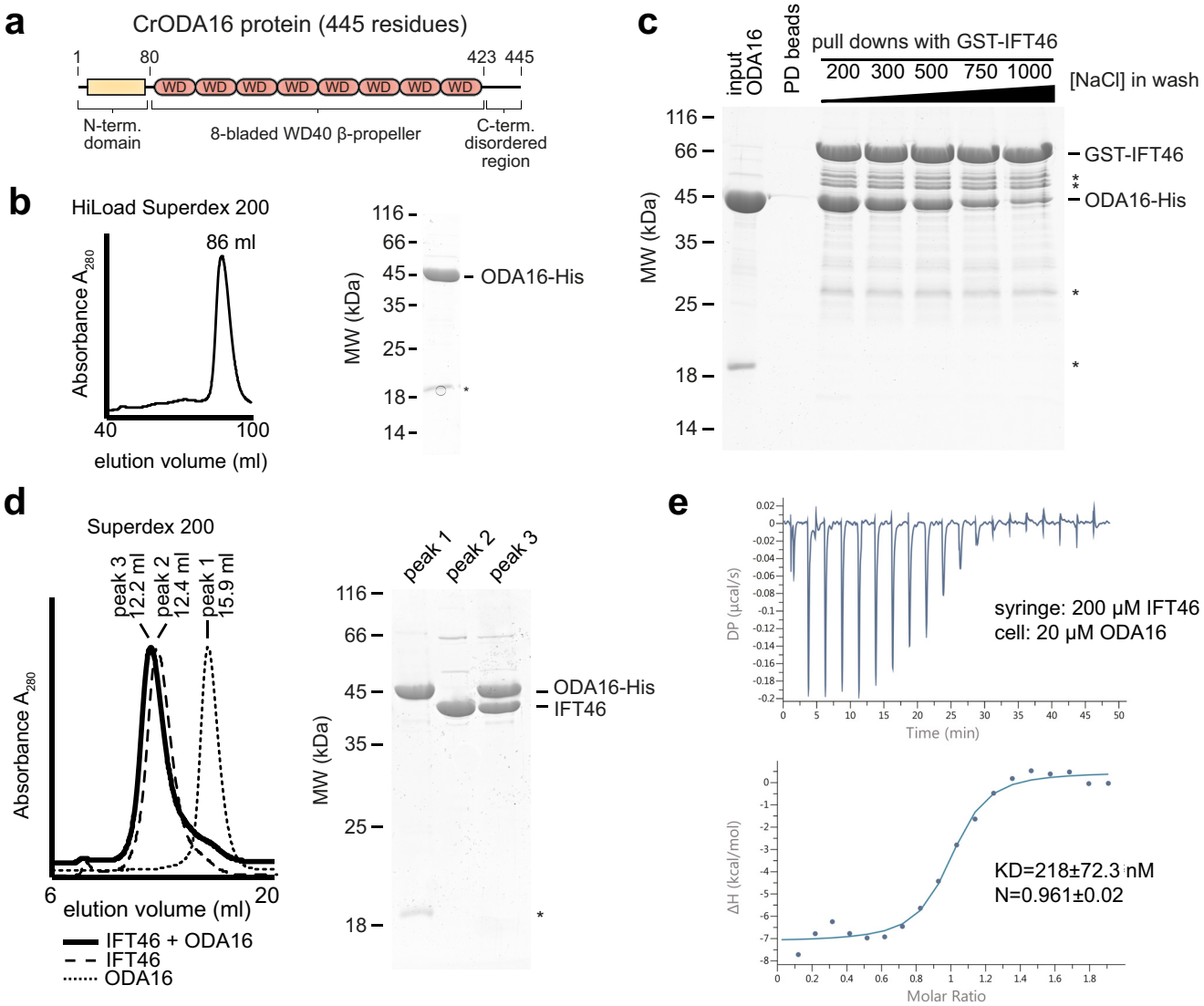

Figure 1. Purified ODA16 forms a stable complex with IFT46. The *asterisks* in *b–d* represent impurities. *a*, domain architecture of ODA16 reveals a small N-terminal (*N-term.*) domain followed by eight predicted WD repeats and a short disordered C-terminal (*C-term.*) region. *b*, SEC profile (*left panel*) and SDS-PAGE (*right panel*) from the final purification step of CrODA16 recombinantly expressed in insect cells. *c*, pulldown of ODA16 using GST-IFT46 at increasing salt concentrations. The stoichiometric interaction between ODA16 and GST-IFT46 observed at 200 mM NaCl is gradually lost as the NaCl concentration is increased to 1 M. *d*, SEC profiles of IFT46, ODA16, and the ODA16-IFT46 complex and the corresponding SDS-PAGE with the peak fraction from each run. *e*, ITC of ODA16 with IFT46 reveals a stoichiometric complex with a K_d of 218 nM. *MW*, molecular mass.

ODA16 β-propeller is the ribosome biogenesis factor RSA4 (38), which interestingly also has a small but structurally divergent domain positioned on the N-terminal face of the β-propeller (Fig. 3*c*).

The relative positions of the two ODA16 domains create a pronounced interdomain cleft with dimensions of ~20 × 20 × 10 Å^3 (Fig. 4, *a* and *b*). This cleft is relatively well conserved, lined by a mixture of hydrophobic and hydrophilic residues and constitutes a potential protein-protein interaction site. A second highly conserved surface patch is found on the C-terminal face of the β-propeller (Fig. 4*c*). This conserved patch is mostly acidic in nature and overlaps with the protein interaction interface of structurally similar β-propellers found in proteins such as the Fbw7 subunit of a cyclin E ubiquitin ligase complex (Fig. 4, *c* and *d*) (39). Both the interdomain cleft and the C-terminal β-propeller surface of ODA16 constitute likely interaction interfaces for IFT46 and ODAs.

Both N- and C-terminal domains of ODA16 are required for ODA16-IFT46 complex formation

To assess whether IFT46 binds to the conserved acidic patch located on the C-terminal side of the ODA16 β-propeller, GST-IFT46 was used to pull down fl ODA16 or any of three different ODA16 constructs lacking either the N-terminal domain (residues 80–445, ODA16ΔN), the C-terminal unstructured tail (residues 1–423, ODA16ΔC), or both (residues 80–423, ODA16ΔNΔC) (see schematics in Fig. 5*a*). The results of this experiment revealed that the N-terminal domain of ODA16 but not the C-terminal unstructured tail is required for interaction with IFT46 (Fig. 5*b*). Given that ODA16N is required for the interaction with IFT46, it appears unlikely that the C-terminal conserved patch of the ODA16 β-propeller, located more than 20 Å away from ODA16N, constitutes the interaction interface for IFT46. To test whether ODA16N is sufficient for the inter-

Downloaded from http://www.jbc.org/ at Helmholtz Zentrum Muenchen - Zentralbibliothek on June 13, 2017

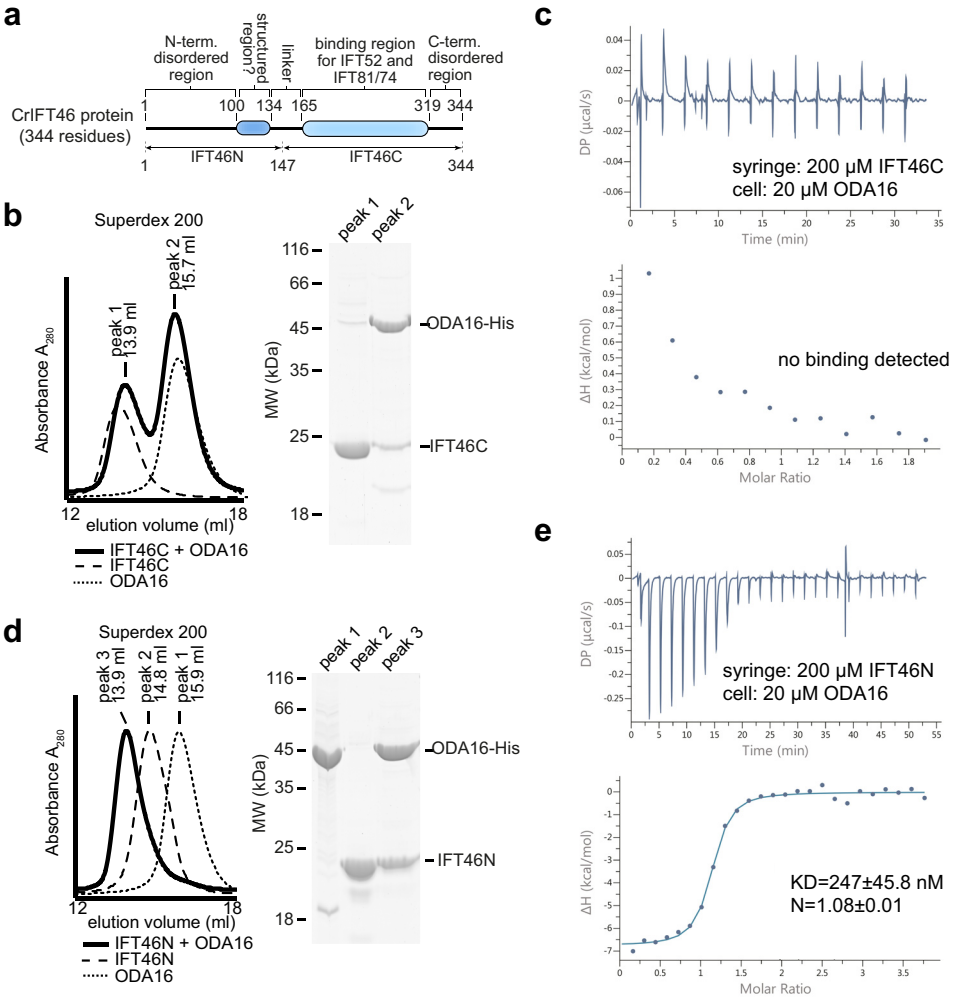

Figure 2. ODA16 interacts with the N-terminal 147 amino acids of IFT46. *a*, domain architecture of CrIFT46. The regions interacting with other IFT proteins are indicated above, and the residues of IFT46N and IFT46C constructs indicated below the domain architecture. *b*, SEC profile of IFT46C incubated with ODA16 does not suggest a stable complex. The small amount of IFT46C present in *peak 2* on the SDS-PAGE is due to overlap between the IFT46C and ODA16 peaks. *c*, ITC of ODA16 with IFT46C demonstrates no detectable interaction between the two proteins. *d*, SEC profile of ODA16 incubated with IFT46N and resulting SDS-PAGE are consistent with a stable stoichiometric complex. *e*, ITC of ODA16 with IFT46N demonstrates a stoichiometric complex with a K_d of 247 nM, similar to ODA16-IFT46. *C-term.*, C-terminal; *N-term.*, N-terminal; *MW*, molecular mass; *DP*, differential power; ΔH, enthalpy changes.

action with IFT46, GST-tagged IFT46 was used in pulldown assays with ODA16N, which showed no detectable interaction (Fig. 5*c*). Both ODA16N and ODA16C domains are thus required for the association with IFT46. To test whether ODA16N and ODA16ΔN have to be covalently attached to mediate IFT46 interaction, GST-IFT46 was incubated with a mixture of purified ODA16N and ODA16ΔN in *trans*, which did also not result in any detectable interaction (Fig. 5*c*). Given that only few interdomain interactions dictate the relative position of ODA16N and the ODA16 β-propeller (Fig. 3*b*), the requirement of covalently attached ODA16N and ODA16ΔN for the association with IFT46 suggests that the interdomain cleft may constitute the IFT46 binding site.

To gain structural insights into the ODA16-IFT46 complex, SEC combined with small-angle X-ray scattering (SEC-SAXS) was used to obtain solution scattering data for ODA16 alone as well as in complex with IFT46N (Table 2 and Fig. 6, *a* and *b*). The pair distance distribution functions in Fig. 6*c* show that the maximum distance between scattering points (D_{max}) increases from ~8 to ~13 nm when ODA16 associates with IFT46N, suggesting a complex with an elongated shape. Envelopes calculated from the SAXS data revealed that the ODA16-IFT46N complex has significant extra density extending along the axis of the N- and C-terminal ODA16 domains (Fig. 6, *d* and *e*). This result indicates that IFT46N binds close to the N-terminal ODA16 domain consistent with the biochemical data shown in Fig. 5. Based on the biochemical and structural data, we conclude that the N-terminal region of IFT46 associates with the N-terminal region of the ODA16 molecule in an interaction where both the N- and C-terminal domains of ODA16 are required for ODA16-IFT46 complex formation.

ODAs bind to the β-propeller of ODA16

To investigate how ODAs interact with ODA16, we first wanted to confirm that we can detect such an interaction in pulldown assays. Flagella were isolated from *C. reinhardtii* cultures and subsequently fractionated to obtain an axonemal extract enriched in ODAs. When a GST-IFT46-ODA16 complex was used as bait, several outer dynein-arm components were efficiently enriched, as confirmed by mass-spectrometric

Downloaded from http://www.jbc.org/ at Helmholtz Zentrum Muenchen - Zentralbibliothek on June 13, 2017

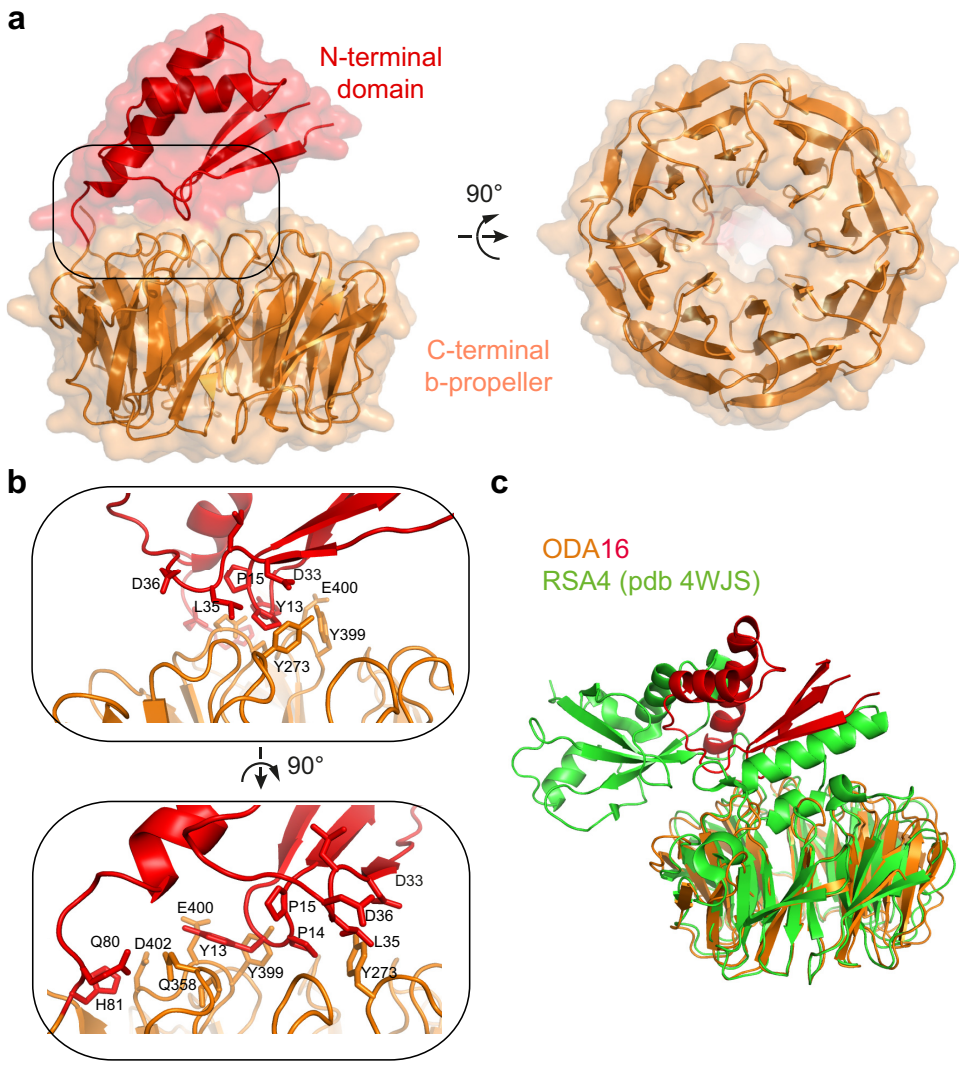

Figure 3. 2.4 Å resolution crystal structure of CrODA16. *a*, cartoon representation of the ODA16 crystal structure with a semitransparent surface is displayed. The 80-residue N-terminal domain is colored *red*, and the C-terminal 8-bladed β-propeller is *orange*. The 90° rotation around the *x* axis is shown on the *right* and provides a view of the C-terminal face of the β-propeller. *b*, zoom-in on the *boxed area* from *a* shows the interacting residues constituting the interdomain interface of ODA16 in two perpendicular orientations rotated around the *vertical axis*. *c*, ODA16 superposed with RSA4 shows that both eight-bladed β-propellers have an N-terminal domain located on top of the N-terminal face of the propellers.

analysis (nano-LC-MS/MS), as well as immunoblotting with anti-IC2 antibodies (supplemental Fig. S3). Furthermore, subunits of the inner dynein arms, IFT particles, IFT motors, radial spokes, docking complex, tubulins, and flagellar-associated proteins were identified in the MS experiments (supplemental Fig. S3), indicating that the GST-tagged IFT46 construct assembles into larger IFT complexes together with factors present in the extract. To investigate the interaction between ODA16 and ODAs more directly, as well as to test for the contributions of ODA16 domains to this interaction, we used various His-tagged versions of ODA16 for pulldowns from axonemal flagellar extract, followed by immunoblotting for the IC2 subunit of ODAs. Although both the full-length and the isolated β-propeller constructs co-precipitated significant amounts of IC2, the N-terminal domain alone did not (Fig. 7*a*). This result shows that the ODA binding site resides in the ODA16 subunit and is not formed by association of ODA16 with IFT46, a possibility we could not rule out in the pulldown with GST-IFT46-ODA16 as bait (supplemental Fig. S3). Furthermore, whereas both the N terminus and the β-propeller of ODA16 are required for the interaction with IFT46 in the IFT complex, only the β-propeller is necessary for binding to an as-of-yet-unidentified component of ODAs. Given that this domain contains highly conserved surface residues, which in structurally related proteins are responsible for direct protein-protein interactions (Fig. 4, *c* and *d*), it is tempting to speculate that ODA16-ODA binding occurs via a similar mechanism. Future experiments should be aimed at identifying the direct ODA16 interaction partner and determining the structural basis for their association.

Discussion

Here we provide structural insights into the IFT of outer dynein arms during flagellar assembly by dissecting interactions within the IFT46-ODA16-ODA protein complex. IFT46 is a core member of the IFT-B1 complex and is required for IFT complex formation (19, 33, 40) through the association of its C-terminal domain with IFT52 (Fig. 7*b*). The region containing

Downloaded from http://www.jbc.org/ at Helmholtz Zentrum Muenchen - Zentralbibliothek on June 13, 2017

Table 1
X-ray data collection and refinement statistics
Statistics for the highest-resolution shell are shown in parentheses.

	CrODA16 native data and refinement
Wavelength (Å)	1.000
Resolution range (Å)	49–2.4 (2.48–2.40)
Space group	P61
Unit cell (a, b, c, α, β, γ)	62.8, 62.8, 460.5, 90, 90, 120
Total reflections	244,365 (23291)
Unique reflections	39,781 (3869)
Multiplicity	6.1 (6.0)
Completeness (%)	99.7 (97.1)
Mean $I/\sigma(I)$	7.3 (1.2)
R_{merge}	0.198 (1.19)
$CC_{½}$	0.989 (0.403)
Twinning statistics	
Twin law	h, − h − k, − l
Twin fraction (phenix.refine)	0.31
<I 2>/<I> 2	1.681
<F> 2/<F2>	0.855
< E 2–1 >	0.609
< L >, <L 2>	0.407, 0.232
R_{work}	0.1611
R_{free}	0.2195
Number of non-hydrogen atoms	6810
Macromolecules	6510
Ligands	15
Water	285
Protein residues	825
RMS bonds	0.097
RMS angles	1.2
Ramachandran favored (%)	96.3
Ramachandran outliers (%)	0.24
Clashscore	12.3
Average B-factor	36.10
Macromolecules	36.00
Ligands	54.70
Solvent	36.70

the N-terminal 165 residues of IFT46 is mostly predicted to be disordered (41) (Figs. 2*a* and supplemental Fig. S1), is not required for IFT complex formation (19, 33), and likely protrudes from the IFT complex. We now show that the 147 most N-terminal residues of IFT46 are sufficient for the high affinity interaction with ODA16 (K_d of ~200 nM). The stability of the ODA16-IFT46 complex is similar to what we previously observed for purified IFT subcomplex (31, 33, 34),[4] suggesting that ODA16 could be a stoichiometric subunit of the IFT complex during flagellar assembly. Interestingly, both the small N-terminal domain and the C-terminal β-propeller, but not the very C-terminal 22 residues of ODA16 (only found in the *C. reinhardtii* ODA16 sequence), are required for the association with IFT46. The crystal structure of ODA16, together with SAXS reconstructions of the ODA16-IFT46N complex and biochemical data, suggests that the N-terminal region of IFT46 may associate with the pronounced cleft observed between the N- and C-terminal domains of ODA16 (summarized in Fig. 7*b*). The SAXS reconstruction of the ODA16-IFT46N complex suggests that it adopts an elongated conformation (Fig. 6*c*). Interestingly, although IFT46 is conserved in all organisms that assemble cilia via IFT, the N-terminal region of IFT46 is only well conserved in organisms with motile cilia (42), consistent with a function in ODA16-mediated IFT of ODAs.

Whereas IFT46 binds to the N-terminal face of the ODA16 molecule, we show that ODAs only require the C-terminal

[4] M. Taschner, A. Mourão, M. Awasthi, J. Basquin, and E. Lorentzen, unpublished results.

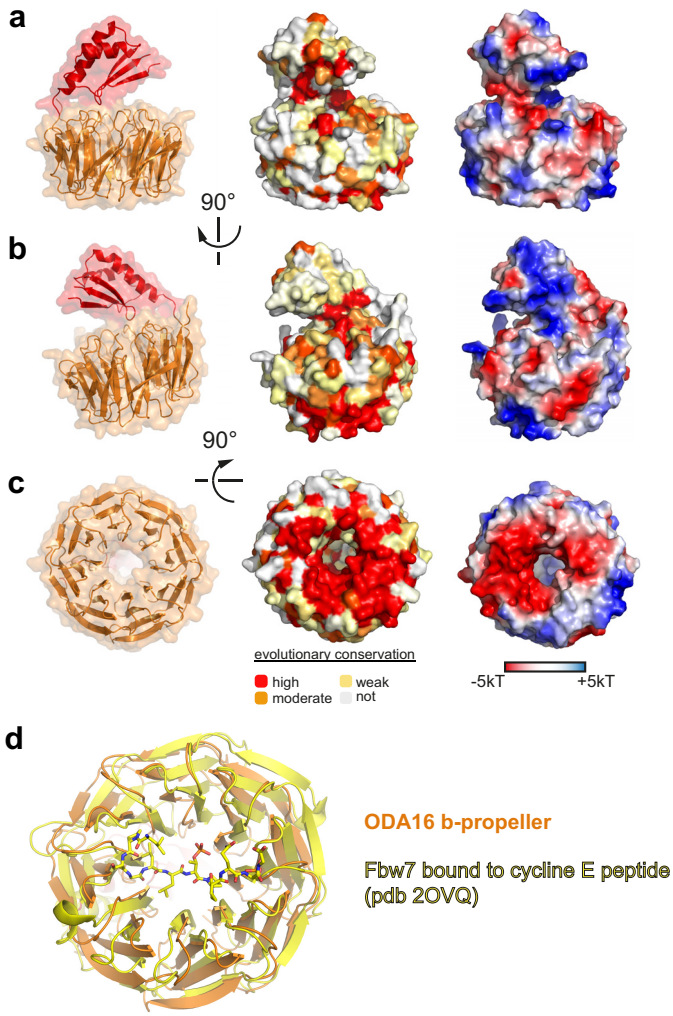

Figure 4. Structure of ODA16 reveals two potential protein-protein interaction sites. *a–c*, cartoon representation (*left panel*), surface conservation (*middle panel*), and electrostatic potential (*right panel*) of three different orientations of the ODA16 crystal structure. *d*, cartoon of the superpositioning of the ODA16 and the Fbw7 structures. The phosphorylated cyclin E peptide bound to the C-terminal face of the Fbw7 structure is shown in *stick* representation.

β-propeller for association with ODA16 (Fig. 7*a*). We observe no direct association between IFT46 and ODAs (data not shown), suggesting that ODA16 is a true cargo adaptor sandwiched between IFT46 and the MDa-sized ODA complexes. However, the observation that some ODAs are still incorporated into the axoneme in the absence of ODA16 suggests that there might be alternative albeit less robust mechanisms of ciliary import of ODAs (16, 18). Although it is difficult to imagine how larger quantities of the MDa-sized ODA complexes enter cilia by diffusion, additional weaker binding sites on IFT components other than IFT46 may result in the ciliary import of smaller quantities of ODAs. Another currently unanswered question is which component(s) of ODAs interact with IFT46. Our pulldown experiments with ODAs extracted from *C. reinhardtii* axonemes do not provide us with any insights into which ODA subunit may be responsible for the binding to ODA16. Also, although it appears likely that the conserved extended patch on the C-terminal face of the ODA16 β-propeller is the interaction surface for ODAs (Fig. 4*c*), this notion

Downloaded from http://www.jbc.org/ at Helmholtz Zentrum Muenchen - Zentralbibliothek on June 13, 2017

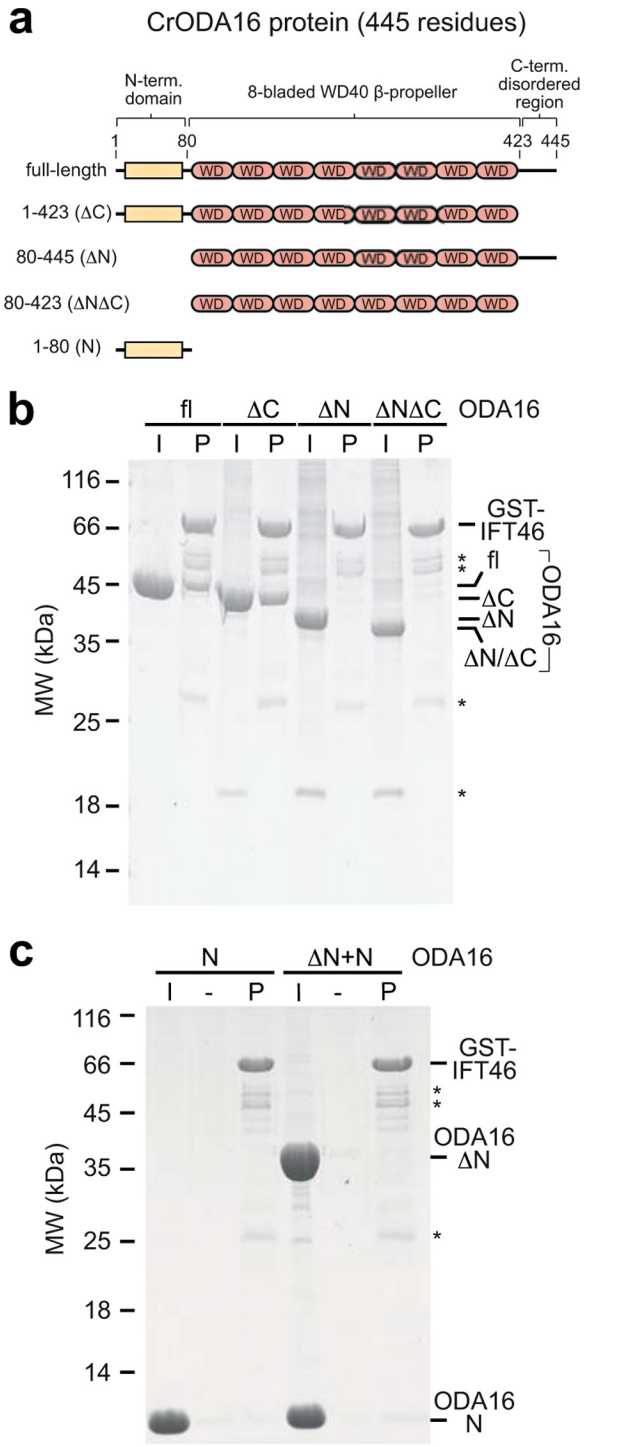

Figure 5. IFT46 association requires both N- and C-terminal domains of ODA16. *a*, schematic representation of the different ODA16 constructs used in this figure. *b*, pulldowns of various ODA16 constructs with GST-IFT46 shows that the N-terminal ODA16 domain, but not the ~25-residue unstructured tail of ODA16, is required for association with IFT46. *c*, neither ODA16N alone nor the N- and C-terminal domains in *trans* are significantly pulled down by GST-IFT46, demonstrating the requirement for covalent attachment of the two ODA16 domains for IFT46 association. *C-term.*, C-terminal; *N-term.*, N-terminal; *MW*, molecular mass.

remains to be proven. Another important unanswered question is how ODAs dissociate from the ODA16-IFT complex at the tip of flagella to allow incorporation into the growing axoneme. Possibly, the remodeling of IFT complexes at the tip of cilia weakens the ODA16-ODA interaction to release the ODA cargoes and allow for axonemal incorporation or such a switch is mediated by as yet unidentified post-translation modification of one or more key players in this process.

Table 2
SAXS data collection

Data-collection parameters			
Instrument:		ESRF BM29	
Wavelength (Å)		0.99	
q-range ($Å^{-1}$)		0.0032 – 0.49	
Sample-to-detector distance		2.867 m	
Exposure time (sec)		1 per frame	
Temperature (K)		277	
Detector		Pilatus 1M (Dectris)	
Flux (photons/s)		1×10^{12}	
Beam size (μm^2)		172 × 172	
Structural parameters		CrODA16	CrODA16/IFT46N
Concentration (mg/mL)		6.0	5.0
From p(r)	Rg (Å)	24.6	31.9
	Dmax (Å)	85.7	132
Porod volume Vp (Å3) $x10^3$		74.6	106.4
Molecular mass (kDa) from Vp		46.6	66.5
Molecular mass (kDa) from sequence		49.2	65.2
Modeling			
Dammif	NSD	0.635	0.487

An important question in cilia biology is how large amounts of axonemal components are transported along cilia to their assembly site at the ciliary tip and how all these factors are bound by the large, but still limited, surface of the multisubunit IFT complex. Whereas it is conceivable that less abundant cargoes share individual binding sites, those that are required in large amounts during ciliary/flagellar assembly (*e.g.* tubulin dimers, axonemal motors, radial spokes, etc.) should have their own dedicated attachment points (42, 43). We and others have previously shown that tubulin dimers are transported by association with a binding module formed by the N-terminal domains of IFT81 and IFT74 (Fig. 7*b*) (22, 26). Another tubulin-binding domain was shown to be located at the N terminus of IFT54 (31), but its exact function during ciliogenesis *in vivo* remains to be determined. Accumulating evidence points to dedicated binding sites for inner dynein arm subunits in the IFT subunits IFT56 (44) and IFT57 (45), based on the analysis of the flagellar proteome from respective *Chlamydomonas* mutants (Fig. 7*b*). Biochemical studies will be necessary to confirm such interactions *in vitro*. Taken together, our understanding of the interactions between the IFT complex and abundant ciliary cargoes has increased significantly in the past few years, but future studies will be necessary to determine the underlying biochemical and structural basis of efficient IFT-mediated ciliogenesis.

Experimental procedures

Cloning, expression, and purification of CrODA16 constructs

The CrODA16 open reading frame was obtained by PCR amplification from a *C. reinhardtii* cDNA library. Sequences encoding the full-length protein or the various N- and C-terminal truncations were amplified with addition of a C-terminal hexahistidine tag, as well as a 5′ BamHI and a 3′ HindIII recog-

Downloaded from http://www.jbc.org/ at Helmholtz Zentrum Muenchen - Zentralbibliothek on June 13, 2017

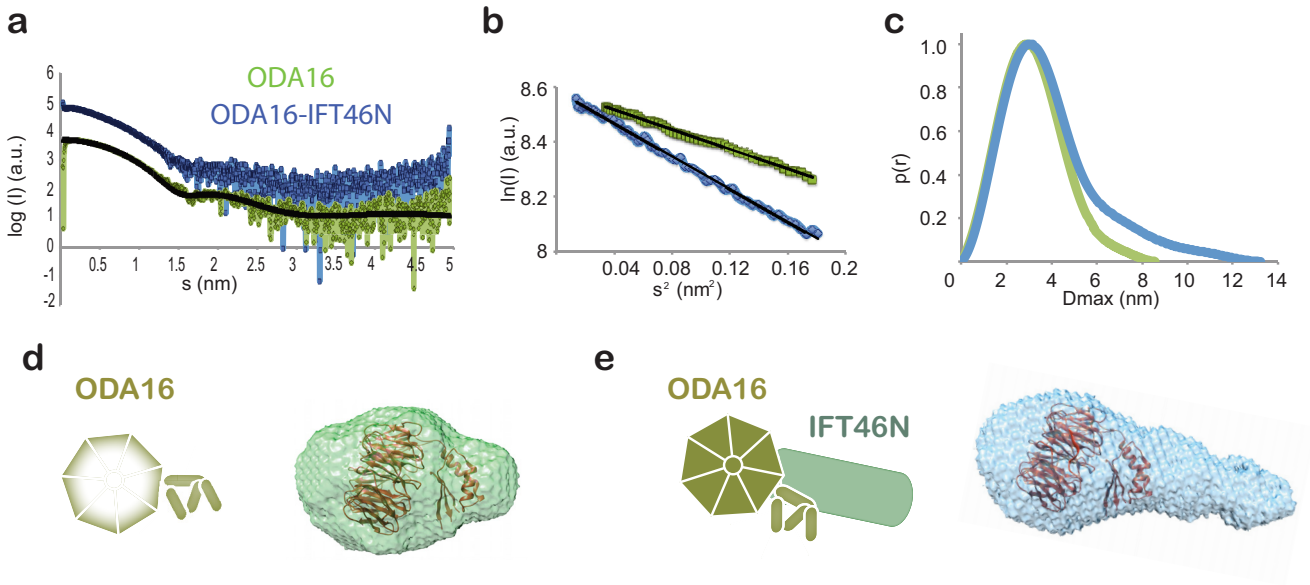

Figure 6. SAXS reconstructions reveal an elongated ODA16-IFT46N complex. *a*, experimental solution scattering curves of ODA16 (*green*) and ODA16-IFT46N (*blue*). *b*, Guinier plot region for the SAXS data of ODA16 (*green*) and ODA16-IFT46N (*blue*). *c*, distance distribution function of the SEC-SAXS profile for ODA16 (*green*) and ODA16-IFT46N (*blue*). *d*, cartoon representation of ODA16 and *ab initio* reconstruction of the ODA16 envelope fitted to ODA16 crystal structure. *e*, cartoon representation of ODA16-IFT46N and *ab initio* reconstruction of the ODA16-IFT46N envelope fitted to the ODA16 crystal structure.

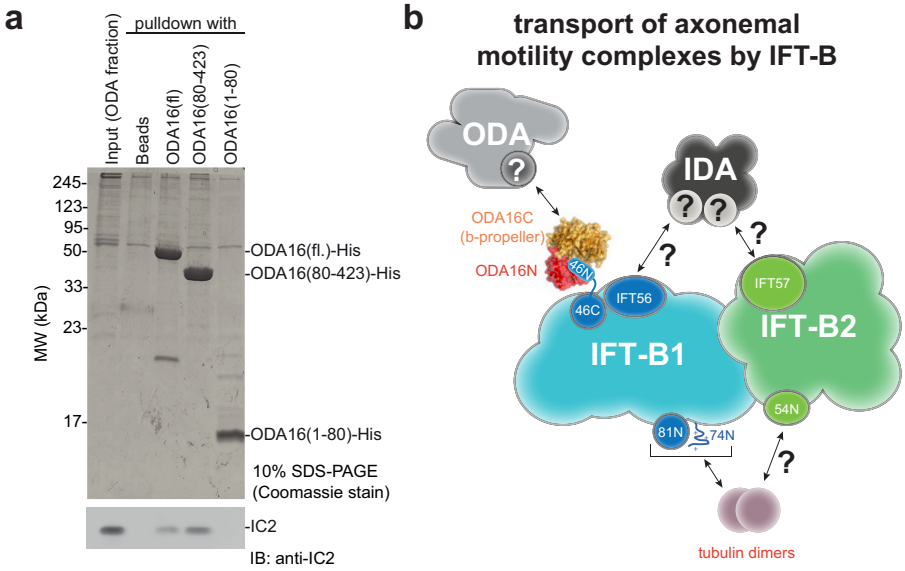

Figure 7. ODAs interact with the ODA16 C-terminal β-propeller. *a*, pulldowns from *C. reinhardtii* flagellar axoneme fractions with different His-tagged constructs of ODA16 show that the ODA16 β-propeller domain is sufficient for the interaction with axonemal outer dynein arms. The *top panel* shows a Coomassie-stained SDS gel of input and pulldowns, and the *bottom panel* is a Western blot for the ODA component IC2. *b*, schematic overview of interactions between components of the IFT complex and various flagellar axonemal components (tubulin dimers, ODAs, and inner dynein arms). *IB*, immunoblot; *IDA*, inner dynein arm; *MW*, molecular mass.

nition sequence, and cloned into MCS2 of the pFL vector (46) between BamHI and HindIII restriction sites. The resulting plasmid was transformed into DH10Bac competent cells, and recombinant baculovirus was produced in Sf21 cells exactly as described previously (31). The virus was then used to infect large volumes (typically 3–6 liters) of HighFive cells at a density of 10^6 cells/ml and incubated for 3 days at 26 °C. The cells were harvested, resuspended in lysis buffer (50 mM Tris-HCl, pH 7.5, 500 mM NaCl, 10% glycerol, 5 mM β-mercaptoethanol, 1× complete protease inhibitor mixture (Roche), 10 μg/ml DNaseI), and sonicated to open the cells (VS70T sonication tip, 40% amplitude, 1 s on and then 2 s off; total energy typically 8–10 kJ). The lysate was clarified by centrifugation at 75,000 × *g* for 45 min, and the supernatant was incubated with 3 ml of nickel-nitrilotriacetic acid resin (Roche) for 2 h at 4 °C. The resin was then collected and washed three times in lysis buffer, and the bound material was recovered by incubation with 35 ml of elution buffer (20 mM Tris, pH 7.5, 200 mM NaCl, 10% glycerol, 500 mM imidazole, pH 7.5). The obtained eluate was passed through a 5-ml ion-exchange column (Q-Sepharose HP), and the flow-through was concentrated and loaded onto a HiLoad Superdex200 SEC column in SEC buffer (10 mM HEPES-KOH, pH

Downloaded from http://www.jbc.org/ at Helmholtz Zentrum Muenchen - Zentralbibliothek on June 13, 2017

7.5, 200 mM NaCl). Finally, peak fractions were analyzed by SDS-PAGE, and fraction containing the protein at sufficient purity were pooled and concentrated and then either used immediately or snap-frozen in aliquots in liquid nitrogen for future use.

Cloning, expression, and purification of CrIFT46 constructs

CrIFT46 constructs were amplified and cloned into the pEC vector series for bacterial expression (with N-terminal His_6/GST/TEV or His_6/TEV tags) as described in previously (33, 34). BL21(DE3) *Escherichia coli* cells were transformed with the resulting plasmids and grown (typically as 2 liter cultures) to an A_{600} of 1.0 at 37 °C. The temperature was then reduced to 18 °C, and expression was achieved by the addition of 0.5 mM isopropyl β-D-thiogalactopyranoside and incubation in a shaker at 18 °C overnight. The cells were harvested by centrifugation and resuspended in 2 pellet volumes of lysis buffer (50 mM Tris-HCl, pH 7.5, 150 mM NaCl, 10% glycerol, 5 mM β-mercaptoethanol, 10 μg/ml DNaseI, 1 mM PMSF). Cell lysis and protein purification were performed exactly as described for other IFT complexes (47). To obtain GST-tagged IFT46 for pulldowns, the elution from the nickel-nitrilotriacetic acid column was concentrated and subjected to SEC.

GST-affinity pulldowns

200 μl of 10 μM GST-tagged IFT46 protein was immobilized on 15 μl of GSH-affinity resin in binding buffer (20 mM Tris-HCl, pH 7.5, 200 mM NaCl, 5% glycerol, 1 mM DTT). When necessary, resin was incubated only with buffer to check for nonspecific interaction of the prey (ODA16 full-length protein or truncation) with the beads. After 2 h of incubation at 4 °C on a rotating wheel, the resin was collected by centrifugation (500 × g, 4 °C) and washed once with binding buffer. For each pulldown reaction, the prey was diluted to a concentration of 10 μM in a total volume of 200 μl with binding buffer, and an input sample was removed for SDS-PAGE analysis. The prey dilution was added to the washed resin, the volume was adjusted to a final volume of 500 μl, and binding was allowed to occur at 4 °C on a rotating wheel for 2 h. The resin was then collected by centrifugation and washed three times using binding buffer supplemented with higher concentrations of NaCl as required for this experiment. Finally, the bound material was eluted by incubation with 40 μl of binding buffer supplemented with 20 μM reduced glutathione. Input and elution samples were then analyzed by SDS-PAGE, and the gel was stained with Coomassie solution.

Interaction analysis using ITC

ITC experiments were done using a Microcal PEAQ-ITC calorimeter (Malvern). Both IFT46 and ODA16 proteins were in a buffer containing 10 mM HEPES, pH 7.5, 100 mM NaCl, and 5% glycerol. A volume of 200 μl of ODA16 at a concentration of 20 μM was titrated with different IFT46 protein constructs at a concentration of 200 μM at 25 °C. For each ITC experiment, a background curve consisting of the titration of the same IFT46 sample into buffer was subtracted to account for heat generated by dilution. Each experiment was carried out in triplicates. The program MicroCal PEAQ-ITC provided by Malvern was used to analyze all ITC data.

Crystallization of ODA16

Full-length CrODA16 at a concentration of 10 mg/ml in a buffer containing 10 mM HEPES, 500 mM NaCl, and 1 mM DTT was mixed in equal volume of precipitant solution containing 20% PEG 3350, 300 mM ammonium sulfate, and 100 mM Bis-Tris, pH 5.5, and crystallized using the sitting drop vapor diffusion technique. Crystals grew after 2–3 days at 18 °C and were cryo-protected in mother liquor supplemented with 15% glycerol and subsequently flash-cooled in liquid nitrogen.

X-ray diffraction data collection and crystal structure determination

X-ray diffraction data were collected at the Swiss Light Source (Villigen, Switzerland) at the PXII beamline on a Pilatus 6M detector and indexed with the XDS package (48) before scaling with Aimless as part of the CCP4 package (49). The space group appeared to be $P6_122$ at the stage of data scaling, but molecular replacement and refinement revealed the true space group to be $P6_1$ with merohedral twinning (twin law h, −h−k, −l, twin fraction of 0.31 according to phenix.refine; see Table 1 for more twinning statistics). Molecular replacement using an eight-bladed β-propeller structure with the highest available sequence identity to ODA16 (RSA4, PDB code 4wjs) gave a clear solution in the program Phaser (50). However, because of the high 8-fold pseudosymmetry within the β-propeller, the molecular replacement solution had to be turned by "two blades" for successful structure solution. The N-terminal domain placed on top of the β-propeller was built manually in Coot (51) followed by refinement in PHENIX (52). Refinement in space group $P6_1$ including the twin law in PHENIX resulted in an R_{free} 7.5% points lower than for refinement in the higher symmetry $P6_122$ space group. The data and refinement statistics are listed in Table 1.

Small-angle X-ray scattering of ODA16 and ODA16-IFT46N

SAXS experiments on ODA16 or the ODA16-IFT46N complex were performed at the BM29 Beamline (European Synchrotron Radiation Facility, Grenoble, France) using a Pilatus 1M detector using a similar protocol the one used previously (53). In brief, SAXS data were collected on proteins and protein complexes eluting directly from a Superdex 200 10/300 GL SEC column. Radiation damage, data merging, and buffer subtraction were performed on site and later verified manually using the program PRIMUS (54). All SAXS parameters such as maximum particle size (D_{max}) were extracted using GNOME (55) from the ATSAS package software (56). Theoretical SAXS curves were calculated from crystal structures using CRYSOL (57) and fitted to the experimental data. *Ab initio* models of ODA16 and ODA16-IFT46N were calculated using the bead-modeling program DAMMIN (58) to generate 10 independent reconstructions. SUPCOMB (59) and DAMAVER (60) were employed to generate the average representative models shown in Fig. 6*e*.

Downloaded from http://www.jbc.org/ at Helmholtz Zentrum Muenchen - Zentralbibliothek on June 13, 2017

Flagellar isolation and fractionation

Chlamydomonas flagella were isolated from 8 liters of initial culture grown in the Tris acetate phosphate medium using the pH shock method (61). To obtain the outer dynein arm fraction, purified flagella were resuspended in HMDEK buffer (30 mM HEPES, 5 mM $MgSO_4$, 1 mM DTT, 0.5 mM EGTA, 25 mM KCl), snap frozen in liquid nitrogen, and then allowed to thaw at room temperature (62). After three consecutive freeze-thaw cycles, flagella were pelleted by centrifugation at 10,000 rpm for 10 min. Supernatants was removed, and the pellets constituting the axonemes were resuspended in HMDE (30 mM HEPES, 5 mM $MgSO_4$, 1 mM DTT, 0.5 mM EGTA) buffer containing 0.6 M NaCl. After 30 min of incubation on ice, the salt-extracted fraction enriched in flagellar ODAs were separated from axonemes by centrifugation at 13,000 rpm for 20 min and dialyzed overnight in HMDE buffer containing 30 mM NaCl.

Proteomics

For each pulldown reaction, flagellar outer dynein arm fraction was used as an input. SEC-purified GST-IFT46 in combination with untagged ODA16 and His-tagged $ODA16_{(fl)}$, $ODA16_{(80-423)}$, and $ODA16_{(1-80)}$ were used as baits for GST pulldown and Ni^{2+} pulldown, respectively. Recombinant GST protein immobilized on GSH-Sepharose beads or Ni^{2+} beads were utilized for negative control experiments. Bait proteins were immobilized on the respective beads by incubating 200 μl of 10 μM protein with a 20-μl bed volume of beads. After incubation for 1 h, the beads were collected, washed thrice with HMDEK buffer, and incubated with *Chlamydomonas* ODA fraction for 4 h at 4 °C on a rotating wheel. GSH or Ni^{2+} resins along with co-precipitated protein complexes were separated by low-speed centrifugation at 400 × *g* for 2 min. The beads were washed twice with cold 20 mM HEPES buffer. Co-precipitated proteins were eluted from GSH beads with GST elution buffer (10 mM Tris-HCl, pH 8, 25 mM reduced glutathione) and from Ni^{2+} beads with HMDEK buffer with 300 mM immidazole. All experiments were performed in triplicate, and elution fractions corresponding to each of the reaction were loaded separately and stacked in a 10% SDS-PAGE gel. Total protein from each lane was digested according to the standard in-gel digestion protocol (63). Digested peptides were purified and concentrated on a C18 StageTip (64) and were analyzed using a Q Exactive HF mass spectrometer (ThermoFisher Scientific). An Easy nLC 1000 system (Thermo Scientific) was used to separate peptides via a 140-min gradient through a column (15-cm column length, 75-μm inner diameter, packed with 1.9-μm beads) maintained at a constant temperature of 45 °C. Raw data were processed using MaxQuant computational platform (65), and statistical analysis was done using the Perseus framework.

Author contributions—M. T. carried out the purification and interaction studies of IFT46 and ODA16 proteins. A. M. carried out SAXS and ITC experiments. J. B. collected all the X-ray diffraction data. M. T. and E. L. determined and refined the ODA16 crystal structure. M. A. carried out all the proteomics experiments, isolated ODAs from flagella, and carried out the ODA16-ODA pulldown. E. L., M. T., M. A., and A. M. wrote the paper.

Acknowledgments—We thank the staff at the Swiss Light Source for help with X-ray diffraction data collection, the staff at the SAXS beamline at EMBL Grenoble for help with SAXS data collection, the crystallization facility of the Max Planck Institute of Biochemistry (Munich, Germany) for access to crystallization screening, and Lissy Weyher and Dr. Nagarjuna Nagaraj (Max Planck Institute of Biochemistry core facility) for mass spectrometric analyses. Furthermore, we are grateful to people in the Department of Structural Cell Biology at the Max Planck Institute of Biochemistry for help with protein expression in insect cells and to Prof. George B. Witman for providing an antibody against the IC2 protein.

References

1. Dobell, C. (1932) *Antony van Leeuwenhoek and his "Little Animals"*, Harcourt: Brace and Company, New York
2. Fliegauf, M., Benzing, T., and Omran, H. (2007) When cilia go bad: cilia defects and ciliopathies. *Nat. Rev. Mol. Cell Biol.* **8,** 880–893
3. Zariwala, M. A., Omran, H., and Ferkol, T. W. (2011) The emerging genetics of primary ciliary dyskinesia. *Proc. Am. Thorac. Soc.* **8,** 430–433
4. Zariwala, M. A., Knowles, M. R., and Omran, H. (2007) Genetic defects in ciliary structure and function. *Annu. Rev. Physiol.* **69,** 423–450
5. Ishikawa, H., and Marshall, W. F. (2011) Ciliogenesis: building the cell's antenna. *Nat. Rev. Mol. Cell Biol.* **12,** 222–234
6. King, S. M. (2016) Axonemal dynein arms. *Cold Spring Harb. Perspect. Biol.* **8,** a028100
7. Fowkes, M. E., and Mitchell, D. R. (1998) The role of preassembled cytoplasmic complexes in assembly of flagellar dynein subunits. *Mol. Biol. Cell.* **9,** 2337–2347
8. Mizuno, N., Taschner, M., Engel, B. D., and Lorentzen, E. (2012) Structural studies of ciliary components. *J. Mol. Biol.* **422,** 163–180
9. Heuser, T., Raytchev, M., Krell, J., Porter, M. E., and Nicastro, D. (2009) The dynein regulatory complex is the nexin link and a major regulatory node in cilia and flagella. *J. Cell Biol.* **187,** 921–933
10. Nicastro, D., McIntosh, J. R., and Baumeister, W. (2005) 3D structure of eukaryotic flagella in a quiescent state revealed by cryo-electron tomography. *Proc. Natl. Acad. Sci. U.S.A.* **102,** 15889–15894
11. Nicastro, D., Schwartz, C., Pierson, J., Gaudette, R., Porter, M. E., and McIntosh, J. R. (2006) The molecular architecture of axonemes revealed by cryoelectron tomography. *Science* **313,** 944–948
12. Ishikawa, T., Sakakibara, H., and Oiwa, K. (2007) The architecture of outer dynein arms in situ. *J. Mol. Biol.* **368,** 1249–1258
13. Kon, T., Oyama, T., Shimo-Kon, R., Imamula, K., Shima, T., Sutoh, K., and Kurisu, G. (2012) The 2.8 Å crystal structure of the dynein motor domain. *Nature* **484,** 345–350
14. Carter, A. P., Cho, C., Jin, L., and Vale, R. D. (2011) Crystal structure of the dynein motor domain. *Science* **331,** 1159–1165
15. Schmidt, H., Zalyte, R., Urnavicius, L., and Carter, A. P. (2015) Structure of human cytoplasmic dynein-2 primed for its power stroke. *Nature* **518,** 435–438
16. Ahmed, N. T., and Mitchell, D. R. (2005) ODA16p, a *Chlamydomonas* flagellar protein needed for dynein assembly. *Mol. Biol. Cell.* **16,** 5004–5012
17. Gao, C., Wang, G., Amack, J. D., and Mitchell, D. R. (2010) Oda16/Wdr69 is essential for axonemal dynein assembly and ciliary motility during zebrafish embryogenesis. *Dev. Dyn.* **239,** 2190–2197
18. Ahmed, N. T., Gao, C., Lucker, B. F., Cole, D. G., and Mitchell, D. R. (2008) ODA16 aids axonemal outer row dynein assembly through an interaction with the intraflagellar transport machinery. *J. Cell Biol.* **183,** 313–322
19. Hou, Y., Qin, H., Follit, J. A., Pazour, G. J., Rosenbaum, J. L., and Witman, G. B. (2007) Functional analysis of an individual IFT protein: IFT46 is required for transport of outer dynein arms into flagella. *J. Cell Biol.* **176,** 653–665
20. Rosenbaum, J. L., and Witman, G. B. (2002) Intraflagellar transport. *Nat. Rev. Mol. Cell Biol.* **3,** 813–825

Downloaded from http://www.jbc.org/ at Helmholtz Zentrum Muenchen - Zentralbibliothek on June 13, 2017

21. Pedersen, L. B., and Rosenbaum, J. L. (2008) Intraflagellar transport (IFT) role in ciliary assembly, resorption and signalling. *Curr. Top. Dev. Biol.* **85,** 23–61
22. Bhogaraju, S., Cajanek, L., Fort, C., Blisnick, T., Weber, K., Taschner, M., Mizuno, N., Lamla, S., Bastin, P., Nigg, E. A., and Lorentzen, E. (2013) Molecular basis of tubulin transport within the cilium by IFT74 and IFT81. *Science* **341,** 1009–1012
23. Bhogaraju, S., Weber, K., Engel, B. D., Lechtreck, K.-F., and Lorentzen, E. (2014) Getting tubulin to the tip of the cilium: one IFT train, many different tubulin cargo-binding sites? *Bioessays* **36,** 463–467
24. Wren, K. N., Craft, J. M., Tritschler, D., Schauer, A., Patel, D. K., Smith, E. F., Porter, M. E., Kner, P., and Lechtreck, K. F. (2013) A differential cargo-loading model of ciliary length regulation by IFT. *Curr. Biol.* **23,** 2463–2471
25. Craft, J. M., Harris, J. A., Hyman, S., Kner, P., and Lechtreck, K. F. (2015) Tubulin transport by IFT is upregulated during ciliary growth by a cilium-autonomous mechanism. *J. Cell Biol.* **208,** 223–237
26. Kubo, T., Brown, J. M., Bellve, K., Craige, B., Craft, J. M., Fogarty, K., Lechtreck, K. F., and Witman, G. B. (2016) Together, the IFT81 and IFT74 N-termini form the main module for intraflagellar transport of tubulin. *J. Cell Sci.* **129,** 2106–2119
27. Cole, D. G., Diener, D. R., Himelblau, A. L., Beech, P. L., Fuster, J. C., and Rosenbaum, J. L. (1998) *Chlamydomonas* kinesin-II-dependent intraflagellar transport (IFT): IFT particles contain proteins required for ciliary assembly in *Caenorhabditis elegans* sensory neurons. *J. Cell Biol.* **141,** 993–1008
28. Piperno, G., and Mead, K. (1997) Transport of a novel complex in the cytoplasmic matrix of *Chlamydomonas* flagella. *Proc. Natl. Acad. Sci. U.S.A.* **94,** 4457–4462
29. Taschner, M., and Lorentzen, E. (2016) The intraflagellar transport machinery. *Cold Spring Harb. Perspect. Biol.* **8,** a028092
30. Boldt, K., van Reeuwijk, J., Lu, Q., Koutroumpas, K., Nguyen, T.-M., Texier, Y., van Beersum, S. E., Horn, N., Willer, J. R., Mans, D. A., Dougherty, G., Lamers, I. J., Coene, K. L. M., Arts, H. H., Betts, M. J., *et al.* (2016) An organelle-specific protein landscape identifies novel diseases and molecular mechanisms. *Nat. Commun.* **7,** 11491
31. Taschner, M., Weber, K., Mourão, A., Vetter, M., Awasthi, M., Stiegler, M., Bhogaraju, S., and Lorentzen, E. (2016) Intraflagellar transport proteins 172, 80, 57, 54, 38, and 20 form a stable tubulin-binding IFT-B2 complex. *EMBO J.* **35,** 773–790
32. Katoh, Y., Terada, M., Nishijima, Y., Takei, R., Nozaki, S., Hamada, H., and Nakayama, K. (2016) Overall architecture of the intraflagellar transport (IFT)-B complex containing Cluap1/IFT38 as an essential component of the IFT-B peripheral subcomplex. *J. Biol. Chem.* **291,** 10962–10975
33. Taschner, M., Kotsis, F., Braeuer, P., Kuehn, E. W., and Lorentzen, E. (2014) Crystal structures of IFT70/52 and IFT52/46 provide insight into intraflagellar transport B core complex assembly. *J. Cell Biol.* **207,** 269–282
34. Taschner, M., Bhogaraju, S., Vetter, M., Morawetz, M., and Lorentzen, E. (2011) Biochemical mapping of interactions within the intraflagellar transport (IFT) B core complex: IFT52 binds directly to four other IFT-B subunits. *J. Biol. Chem.* **286,** 26344–26352
35. Lucker, B. F., Miller, M. S., Dziedzic, S. A., Blackmarr, P. T., and Cole, D. G. (2010) Direct interactions of intraflagellar transport complex B proteins IFT88, IFT52, and IFT46. *J. Biol. Chem.* **285,** 21508–21518
36. Moon, T. M., Correa, F., Kinch, L. N., Piala, A. T., Gardner, K. H., and Goldsmith, E. J. (2013) Solution structure of the WNK1 autoinhibitory domain, a WNK-specific PF2 domain. *J. Mol. Biol.* **425,** 1245–1252
37. Voorhees, R. M., Fernández, I. S., Scheres, S. H., and Hegde, R. S. (2014) Structure of the mammalian ribosome-Sec61 complex to 3.4 Å resolution. *Cell.* **157,** 1632–1643
38. Bassler, J., Paternoga, H., Holdermann, I., Thoms, M., Granneman, S., Barrio-Garcia, C., Nyarko, A., Lee, W., Stier, G., Clark, S. A., Schraivogel, D., Kallas, M., Beckmann, R., Tollervey, D., Barbar, E., *et al.* (2014) A network of assembly factors is involved in remodeling rRNA elements during preribosome maturation. *J. Cell Biol.* **207,** 481–498
39. Hao, B., Oehlmann, S., Sowa, M. E., Harper, J. W., and Pavletich, N. P. (2007) Structure of a Fbw7-Skp1-cyclin E complex: multisite-phosphorylated substrate recognition by SCF ubiquitin ligases. *Mol. Cell* **26,** 131–143
40. Richey, E. A., and Qin, H. (2012) Dissecting the sequential assembly and localization of intraflagellar transport particle complex B in *Chlamydomonas*. *PLoS One* **7,** e43118
41. Taschner, M., Bhogaraju, S., and Lorentzen, E. (2012) Architecture and function of IFT complex proteins in ciliogenesis. *Differentiation* **83,** S12–S22
42. Bhogaraju, S., Engel, B. D., and Lorentzen, E. (2013) Intraflagellar transport complex structure and cargo interactions. *Cilia* **2,** 10
43. Lechtreck, K. F. (2015) IFT-cargo interactions and protein transport in cilia. *Trends Biochem. Sci.* **40,** 765–778
44. Ishikawa, H., Ide, T., Yagi, T., Jiang, X., Hirono, M., Sasaki, H., Yanagisawa, H., Wemmer, K. A., Stainier, D. Y., Qin, H., Kamiya, R., and Marshall, W. F. (2014) TTC26/DYF13 is an intraflagellar transport protein required for transport of motility-related proteins into flagella. *Elife* **3,** e01566
45. Jiang, X., Hernandez, D., Hernandez, C., Ding, Z., Nan, B., Aufderheide, K., and Qin, H. (2017) IFT57 stabilizes assembled intraflagellar transport complex and mediates transport of motility-related flagellar cargo. *J. Cell Sci.* **130,** 879–891
46. Bieniossek, C., Richmond, T. J., and Berger, I. (2008) MultiBac: multigene baculovirus-based eukaryotic protein complex production. *Curr. Protoc. Protein Sci.* Chapter 5, Unit 5.20
47. Taschner, M., and Lorentzen, E. (2016) Recombinant reconstitution and purification of the IFT-B core complex from *Chlamydomonas reinhardtii*. *Methods Mol. Biol.* **1454,** 69–82
48. Kabsch, W. (2010) XDS. XDS. *Acta Crystallogr. D Biol. Crystallogr.* **66,** 125–132
49. Winn, M. D., Ballard, C. C., Cowtan, K. D., Dodson, E. J., Emsley, P., Evans, P. R., Keegan, R. M., Krissinel, E. B., Leslie, A. G., McCoy, A., McNicholas, S. J., Murshudov, G. N., Pannu, N. S., Potterton, E. A., Powell, H. R., *et al.* (2011) Overview of the CCP4 suite and current developments. *Acta Crystallogr. D Biol. Crystallogr.* **67,** 235–242
50. Storoni, L. C., McCoy, A. J., and Read, R. J. (2004) Likelihood-enhanced fast rotation functions. *Acta Crystallogr. D Biol. Crystallogr.* **60,** 432–438
51. Emsley, P., Lohkamp, B., Scott, W. G., and Cowtan, K. (2010) Features and development of Coot. *Acta Crystallogr. D Biol. Crystallogr.* **66,** 486–501
52. Adams, P. D., Afonine, P. V., Bunkóczi, G., Chen, V. B., Davis, I. W., Echols, N., Headd, J. J., Hung, L.-W., Kapral, G. J., Grosse-Kunstleve, R. W., McCoy, A. J., Moriarty, N. W., Oeffner, R., Read, R. J., Richardson, D. C., *et al.* (2010) PHENIX: a comprehensive Python-based system for macromolecular structure solution. *Acta Crystallogr. D Biol. Crystallogr.* **66,** 213–221
53. Brennich, M. E., Round, A. R., and Hutin, S. (2017) Online size-exclusion and ion-exchange chromatography on a SAXS beamline. *J. Vis. Exp.* 10.3791/54861
54. Konarev, P. V., Volkov, V. V., Sokolova, A. V., Koch, M. H., and Svergun, D. I. (2003) PRIMUS: a Windows PC-based system for small-angle scattering data analysis. *J. Appl. Crystallogr.* **36,** 1277–1282
55. Svergun, D. I. (1992) Determination of the regularization parameter in indirect-transform methods using perceptual criteria. *J. Appl. Crystallogr.* **25,** 495–503
56. Petoukhov, M. V., Franke, D., Shkumatov, A. V., Tria, G., Kikhney, A. G., Gajda, M., Gorba, C., Mertens, H. D., Konarev, P. V., and Svergun, D. I. (2012) New developments in the ATSAS program package for small-angle scattering data analysis. *J. Appl. Crystallogr.* **45,** 342–350
57. Svergun, D., Barberato, C., and Koch, M. H. (1995) CRYSOL: a program to evaluate X-ray solution scattering of biological macromolecules from atomic coordinates. *J. Appl. Crystallogr.* **28,** 768–773
58. Svergun, D. I. (1999) Restoring low resolution structure of biological macromolecules from solution scattering using simulated annealing. *Biophys. J.* **76,** 2879–2886
59. Kozin, M. B., and Svergun, D. I. (2001) Automated matching of high- and low-resolution structural models. *J. Appl. Crystallogr.* **34,** 33–41
60. Volkov, V. V., and Svergun, D. I. (2003) Uniqueness of ab initioshape determination in small-angle scattering. *J. Appl. Crystallogr.* **36,** 860–864
61. Witman, G. B. (1986) Isolation of *Chlamydomonas* flagella and flagellar axonemes. *Methods Enzymol.* **134,** 280–290

Downloaded from http://www.jbc.org/ at Helmholtz Zentrum Muenchen - Zentralbibliothek on June 13, 2017

ASBMB

62. Rompolas, P., Pedersen, L. B., Patel-King, R. S., and King, S. M. (2007) *Chlamydomonas* FAP133 is a dynein intermediate chain associated with the retrograde intraflagellar transport motor. *J. Cell Sci.* **120,** 3653–3665
63. Shevchenko, A., Tomas, H., Havlis, J., Olsen, J. V., and Mann, M. (2006) In-gel digestion for mass spectrometric characterization of proteins and proteomes. *Nat. Protoc.* **1,** 2856–2860
64. Rappsilber, J., Mann, M., and Ishihama, Y. (2007) Protocol for micro-purification, enrichment, pre-fractionation and storage of peptides for proteomics using StageTips. *Nat. Protoc.* **2,** 1896–1906
65. Cox, J., and Mann, M. (2008) MaxQuant enables high peptide identification rates, individualized p.p.b.-range mass accuracies and proteome-wide protein quantification. *Nat. Biotechnol.* **26,** 1367–1372

Downloaded from http://www.jbc.org/ at Helmholtz Zentrum Muenchen - Zentralbibliothek on June 13, 2017

Structural basis of outer dynein arm intraflagellar transport by the transport adaptor protein ODA16 and the intraflagellar transport protein IFT46

Michael Taschner, André Mourão, Mayanka Awasthi, Jerome Basquin and Esben Lorentzen

J. Biol. Chem. 2017, 292:7462-7473.
doi: 10.1074/jbc.M117.780155 originally published online March 15, 2017

Access the most updated version of this article at doi: 10.1074/jbc.M117.780155

Alerts:
- When this article is cited
- When a correction for this article is posted

Click here to choose from all of JBC's e-mail alerts

Supplemental material:
http://www.jbc.org/content/suppl/2017/03/15/M117.780155.DC1

This article cites 63 references, 24 of which can be accessed free at
http://www.jbc.org/content/292/18/7462.full.html#ref-list-1

Downloaded from http://www.jbc.org/ at Helmholtz Zentrum Muenchen - Zentralbibliothek on June 13, 2017